Carrier mobility reduction and model in n-type compensated silicon

CrossMark

Shuai Li [a], Wenxiu Gao [a], Songsheng Zheng [a], Haoran Cheng [a], Xing Yang [a], Qijin Cheng [a,b,*], Chao Chen [a,*]

[a] College of Energy, Xiamen University, Xiamen City, Fujian Province 361005, PR China
[b] Shenzhen Research Institute of Xiamen University, Shenzhen City, Guangdong Province 518000, PR China

ARTICLE INFO

ABSTRACT

Research on electrical properties of the compensated silicon is very crucial for understanding the doping layer and compensated substrates of solar cells. Regarding the fact that there are still inadequate experimental data of carrier mobility on the n-type compensated silicon, hence in this paper, both majority electron and minority hole mobilities measured on the n-type compensated solar-grade silicon substrates are presented. Prediction models of carrier mobility are essential for material characterization and device (e.g. solar cells) simulation. However, as prediction models of carrier mobility are commonly established based on the uncompensated silicon, large deviations of carrier mobility have been observed on the compensated silicon. In this work, the standard Klaassen's model and optimized model for the compensated silicon by Schindler et al. are reviewed and compared to measured carrier mobilities. Moreover, the factors that lead to deviations of Klaassen's model on the n-type compensated silicon are critically discussed, and then we propose an optimized model for prediction of carrier mobility in the compensated silicon. This model can also be extended to both majority and minority carrier mobilities in p- and n-type compensated silicon and fits well with previous published data as well as carrier mobility data presented here. In addition, evolutions of majority electron and minority hole mobilities as crystal grows are also simulated for n-type compensated Czochralski silicon which agrees well with our measured results.

© 2017 Published by Elsevier B.V.

1. Introduction

Compensated silicon typically contains high concentrations of both donors and acceptors. The compensated silicon has more ionized scattering impurities than the uncompensated silicon for the same carrier concentration. This greater ionized impurity scattering will lead to a significant reduction of both minority and majority carrier mobilities due to compensation [1–7]. As the majority and minority carrier mobilities are directly connected with the resistivity and carrier diffusion length of the substrate, respectively, these two parameters significantly affect the solar cell efficiency. In a semi-physics based carrier mobility model developed by Klaassen, the presence of both acceptors and donors as scattering centers has been taken into account and it unifies the description of majority and minority carrier mobilities by considering impurity scattering, electron-hole scattering, screening by charge carriers, as well as temperature dependence of carrier mobility [8,9]. Thus, the Klaassen's model was commonly used as the standard model of carrier mobility for the uncompensated silicon for

photovoltaic (PV) application [5,10–12]. However, majority hole mobilities measured on the p-type compensated silicon are frequently reported to show large deviations from the Klaassen's model [1,2,5–7,11–16]. Although Fourmond et al. [17] tried to reduce the deviations by adding an empirical correction term according to Matthiesen's rule ($1/\mu = 1/\mu_{Klaassen} + 1/\mu_{cor}$), the physics behind the correction term is still unclear.

Recently, as for compensated silicon, Schindler et al. have developed an optimized model [16]. In this work, deviations of carrier mobility have already been discussed in detail, not only on the base of majority hole mobilities in the p-type compensated silicon, but also on the base of all types of mobilities. Schindler et al. inserted several new parameters in Klaassen's model based on published carrier mobility data on the p-type compensated silicon and kept the physical character of Klaassen's model [16]. About the origin of deviations of Klaassen's model from measured carrier mobilities, Schindler et al. argued that the reduced screening is not sufficiently taken into account in Klaassen' model [16]. Moreover, Forster et al. suggested that there is no compensation-specific mechanism and that the reduced screening alone cannot explain the mobility reduction along the whole temperature range in publications [5,18]. It needs to be pointed out that the above optimizations are both made based on the Klaassen's model, and that the origin

---

* Corresponding authors at: College of Energy, Xiamen University, Xiamen City, Fujian Province 361005, PR China (Q. Cheng).
E-mail addresses: qijin.cheng@xmu.edu.cn (Q. Cheng), cchen@xmu.edu.cn (C. Chen).

of the deviations is still inadequately investigated. These above-mentioned consequences motivate us to investigate the origin of deviations of Klaassen's model and give a new optimized model of carrier mobilities.

Research on the n-type uncompensated silicon as a common solar-grade silicon feedstock for solar cells has been undertaken for a long time [19–24]. Compensated silicon made from metallurgical route and recycling process appears as a cost-effective way to obtain the solar-grade silicon feedstock [20,25,26]. Therefore, it is of great importance to characterize the n-type compensated silicon as substrates of solar cells. Moreover, it is also essential for understanding the contra-doping layer of p-type silicon. However, to the best of our knowledge, very few investigations have been carried out on the characterization of the carrier mobility of the n-type compensated silicon.

Therefore, in this paper we present both electron and hole mobilities measured on the n-type compensated silicon for PV applications. Carrier mobilities obtained from different modelings are compared at a large range of carrier concentrations. Particularly, the discrepancy between Klaassen's model and experimental carrier mobilities is critically discussed in detail. Then a new optimized model is proposed for the n-type compensated silicon with no additional parameters included. We also extend the optimized model to the p-type compensated silicon based on a wide range of published data, and an excellent agreement is obtained. Eventually, evolutions of majority electron and minority hole mobilities are simulated as crystal grows for the n-type compensated Czochralski (Cz) silicon, which agrees well with our measured results.

2. Material preparation and method

The n-type compensated solar-grade silicon feedstock was prepared by metallurgical method. Directional solidification was carried out prior to the Cz crystal growth to get more homogeneous material. In the solar-grade silicon, scattering of carriers by impurities except ionized dopants (boron and phosphorus) is negligible. Then $\langle 1\,0\,0 \rangle$ oriented Cz silicon rods with a diameter of 8 inches were grown at lengths of $130 - 150$ cm. All silicon rods were sliced into 156×156 mm^2 pseudo-squared wafers with a thickness of about 190 μm. Silicon wafers were roughly classified by segregated dopant concentration as crystal grows with the initial dopant concentrations determined by inductively coupled plasma mass spectrometry (ICP-MS) in silicon feedstock. In addition, the total boron or phosphorus dopants in silicon wafers were determined by glow discharge mass spectrometry (GDMS), irrespective of its charge state (ionized or neutral). The concentrations of interstitial oxygen were measured by Fourier transform infrared (FTIR) spectroscopy and controlled under 5×10^{17} cm^{-3}, and then a subsequent thermal donor annihilation process of 300 s (the highest temperature is 650 °C) using rapid thermal processing (RTP) oven under nitrogen ambient was carried out (this thermal donor annihilation process was presented in detail by Pascoa [27]). In this way, less thermal donors were introduced by oxygen [28]. Other impurities were also examined by GDMS. Electro-chemical capacitance voltage (ECV) method was applied to determine the carrier concentration c with an average etched depth of 0.3 μm, and the deviations were controlled below 5% for measurement. Resistivities ρ of wafers were measured by standard four point probe test. Afterwards, majority carrier mobility $\mu_{maj.}$ (i.e. electron mobility μ_e for the n-type silicon) was deduced by formula $\mu_{maj.} = 1/cq\rho$ from the carrier concentration c and resistivity ρ. For comparison, Hall mobility was tested with HMS-5000 Hall effect measurement system with a magnetic field of $0.55T$. Hall mobility could be converted to conductivity mobility by using Hall factors which are

suggested as 1.1 for n-type compensated silicon in publication [29] and 0.72–0.76 for p-type compensated silicon in publications [4,5,11,13,14,30].

Note that quasi-steady state photoconductance (QSSPC) method was not suitable for determination of minority carrier lifetime, for the reason that it involved the uncertain minority carrier mobility in calculation, while for microwave photoconductance decay (MWPCD) method, uncertain carrier mobility was avoided by using transient degradation lifetime. The prepared silicon wafers were double-side polished with a solution of mixture of $HNO_3 : HF : CH_3COOH = 5 : 3 : 3$ and then were dipped into boiling H_2O_2 solution for 10 min. Afterwards, silicon wafers were coated with a layer of Si_3N_4 (the thickness is about 120 nm and the refraction index is about 2.1) on the top surface at a temperature of 150 °C. Effective carrier lifetime (τ_{eff}) was measured by MW-PCD method using WT-2000 at a fixed carrier injection level (photon flux density is about 1×10^{15} cm^{-3}; see Fig. 1). As shown by the red rectangle (the larger one) in Fig. 1, a section of 1 cm × 1 cm was cut from the central area (with a higher effective carrier lifetime) for surface photovoltage (SPV) test. It is worth noting that the effective carrier lifetime τ_{eff} used in our calculation is also an average value of this small section (red rectangle area). The SPV test was undertaken using metal-insulator-semiconductor (MIS) structure which was described in detail in publications [31,32,33]. As mentioned above, the top surface was covered using a dielectric film of Si_3N_4 (insulator), and ohmic contact was prepared on the back surface of Si wafers. The spectral range was of 0.85–1.01 μm when the incident photon flux density was kept constant (identical to MW-PCD test). The effective minority carrier diffusion length (i.e. L_p for n-type silicon) was extracted from the analysis of the spectral data of SPV test.

Then the minority hole mobility in n-type silicon can be obtained using the following expression:

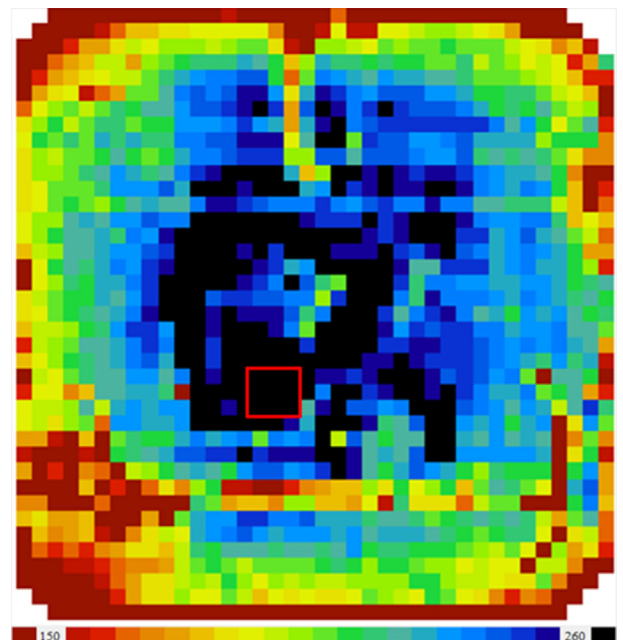$$\mu_p = \frac{L_p^2 q}{kT\tau_{eff}} \tag{1}$$

Fig. 1. Mapping of carrier lifetimes of a wafer by MW-PCD method (the red rectangle in the center shows the area for SPV test). (For interpretation of the references to colour in this figure legend, the reader is referred to the web version of this article.)

where $kT = 0.026$ eV at room temperature. In addition, all of the measurements were carried out under room temperature of 300 ± 1.5 K.

3. Experimental results and discussion

This section presents the experimental majority and minority carrier mobilities for moderately compensated n-type silicon. Carrier mobilities measured on compensated silicon wafers with different concentrations of boron are compared, and three reference uncompensated silicon wafers are used. Concentration of phosphorus in silicon is given by $N_D = N_A + c_{maj}$. Here, N_D is the total concentration of measured phosphorus (P); N_A is the total concentration of measured boron (B); $c_{maj.}$ is the concentration of measured majority carriers. The concentrations of boron ($< 1.4 \times 10^{13}$ cm^{-3}) are negligible in reference uncompensated silicon wafers, while the concentrations of boron are from 2.0×10^{15} cm^{-3} to 2×10^{16} cm^{-3} in n-type compensated silicon wafers investigated in this paper (the corresponding compensation level $C_l = (N_D + N_A)/(N_D - N_A)$ here is from 2.4 to 34.). We measured the electron mobility μ_e and hole mobility μ_h of the n-type compensated silicon wafers, and experimental results are listed in Table S1 in Supporting Information.

3.1. Motivation of modeling and optimized expression

3.1.1. Discrepancy analysis by comparison of different models

Klaassen's model takes into account several contributions to carrier mobility: lattice scattering, donor scattering, acceptor scattering, electron-hole scattering, as well as screening effect, which is physically sufficient to describe scattering cross sections in the compensated silicon [8]. It is generally accepted that the scattering cross section is greater for attractive charged potentials than for repulsive charged potentials [34]. According to JWKB approximation [35,36], the factor $G(P)$ is calculated as the scattering cross section ratio of repulsive screened Coulomb potentials to that of attractive screened Coulomb potentials. And the factor $F(P)$ is the scattering cross section ratio of stationary scattering centers to that of moving scattering centers. In Klaassen's model, it starts from a combination of Conwell-Weisskopf and Brooks-Herring (CW-BH) mobility expression [8]:

$$\mu_{i,j}(N_j, c) = \mu_{i,N}\left(\frac{N_{ref,1}}{N_j}\right)^{\alpha_1} + \mu_{i,c}\left(\frac{c}{N_j}\right) \tag{2}$$

where the subscript j stands for D (donor), A (acceptor) or h (hole); the subscript i stands for e (electrons) or h (holes); $\mu_{i,N}$, $\mu_{i,c}$, $N_{ref,1}$, and α_1 are model parameters in Klaassen's model (see also Ref. [37]).

Instead of using Klaassen's unified model which was proposed for simplification of computational procedure, the contributions of scattering of donors, acceptors and carriers are summed up following Matthiesen's rule as the expression [8,37]:

$$\mu_{i,D+A+h}^{-1} = \mu_{i,D}^{-1} + \mu_{i,A}^{-1} + \mu_{i,h}^{-1} \tag{3}$$

where the subscript i stands for e (electrons) or h (holes); $\mu_{i,D+A+h}$ is carrier mobility due to donor scattering, acceptor scattering and hole scattering; $\mu_{i,D}$ is carrier mobility due to donor scattering; $\mu_{i,A}$ is carrier mobility due to acceptor scattering; and $\mu_{i,h}$ is carrier mobility due to hole scattering. Then by summing up the carrier mobility due to lattice scattering, the calculated total carrier mobility $\mu_{i,Matt.sum}$ following the Matthiesen's rule, which is based on the basic equations in Klaassen's work [8], can be expressed as

$$\mu_{i,Matt.sum}^{-1} = \mu_{i,D+A+j}^{-1} + \mu_{i,L}^{-1} \tag{4}$$

We compare the calculated carrier mobilities by different models and also some of our measured data when concentrations of compensated boron are $< 5.0 \times 10^{13}$ cm^{-3}, 2.0×10^{15} cm^{-3} (0.04 ppma), 1.0×10^{16} cm^{-3} (0.2 ppma) and 2.0×10^{16} cm^{-3} (0.4 ppma), respectively. We involve the carrier mobility calculated by Klaassen's model $\mu_{i,Klaassen}$, the carrier mobility calculated by Schindler's model $\mu_{i,Schindler}$, the carrier mobility calculated by Eq. (4) $\mu_{i,Matt.sum}$, and the carrier mobility $\mu_{i,thiswork}$ calculated by our optimized model (it will be discussed later) in Figs. 2 and 3. The values calculated by different models are identical in the uncompensated silicon, and start to go differently with the increase of the concentration of compensated boron in the compensated silicon.

We can see from Figs. 2 and 3 that commonly accepted Klaassen's model shows very large deviations from measured carrier mobilities. Klaassen calculated carrier mobilities due to all scatterings following Matthiesen's rule before it reached a unified model in his paper [8]. Therefore, we can see from Figs. 2 and 3(a) that the calculated $\mu_{i,Klaassen}$ is same to $\mu_{i,Matt.sum}$ in the uncompensated silicon. However, as illustrated in Figs. 2 and 3(b)–(d), the calculated $\mu_{i,Klaassen}$ goes differently from $\mu_{i,Matt.sum}$ in the compensated silicon. This result suggests that the Klaassen' unified model does not follow the Matthiesen's rule in compensated silicon. In our opinion, this is the first reason that the discrepancy originates. As the parameters in Klaassen's model are fitted based upon measured data on the uncompensated silicon, it is insufficient to describe scatterings of both acceptors and donors when minority impurity is introduced. That is to say, the weighing of $G(P)$ and $F(P)$ factors in Klaassen's model changes for the compensated silicon.

The second reason for the discrepancy originates from the commonly accepted reduced screening effect by carriers [1,2,5,16]. According to the statistical screening theory by Ridley [42], screening is considered by the second term on the right hand side of Eq. (2). Specifically, the majority carrier concentration c in Eq. (2) should reduce to $c = N_D - N_A$ instead of $c = N_D$ for the calculation of screening effect in the n-type compensated silicon. In other words, the reduction of screening effect by compensation is insufficiently taken into account in both calculated mobility by Klaassen's model $\mu_{i,Klaassen}$ and calculated mobility by Eq. (4) $\mu_{i,Matt.sum}$. As a result, carrier mobilities calculated by Eq. (4) $\mu_{i,Matt.sum}$ show deviations from measured data in the compensated silicon (see Figs. 2 and 3).

3.1.2. Optimized expression of carrier mobility model
3.1.2.1. Calculated carrier mobility following Matthiesen's rule $\mu_{i,Matt.sum}$. Based on the Caughey-Thomas expression [43] and approximation of CW-BH theory [44], main scattering cross sections of electrons including screening are deduced using expression as Eq. (2), and the resulting expressions of electron mobilities due to scattering of donors, acceptors and holes in the n-type compensated silicon are as follows [8]:

$$\mu_{e,D}(N_D, c) = \mu_{e,N}\left(\frac{N_{ref,1}}{N_D}\right)^{\alpha_1} + \mu_{e,c}\left(\frac{c}{N_D}\right) \tag{5}$$

$$\begin{aligned} \mu_{e,A}(N_A, c) &= \mu_{e,D}(N_D = N_A, c)/G(P) \\ &= \mu_{e,N}\left(\frac{N_{ref,1}}{N_A}\right)^{\alpha_1}\Big/G(P) + \mu_{e,c}\left(\frac{c}{N_A}\right)/G(P) \end{aligned} \tag{6}$$

$$\begin{aligned} \mu_{e,h}(p, c) &= F(P)\mu_{e,D}(N_D = p, c) \\ &= F(P)\mu_{e,N}\left(\frac{N_{ref,1}}{p}\right)^{\alpha_1} + F(P)\mu_{e,c}\left(\frac{c}{P}\right) \end{aligned} \tag{7}$$
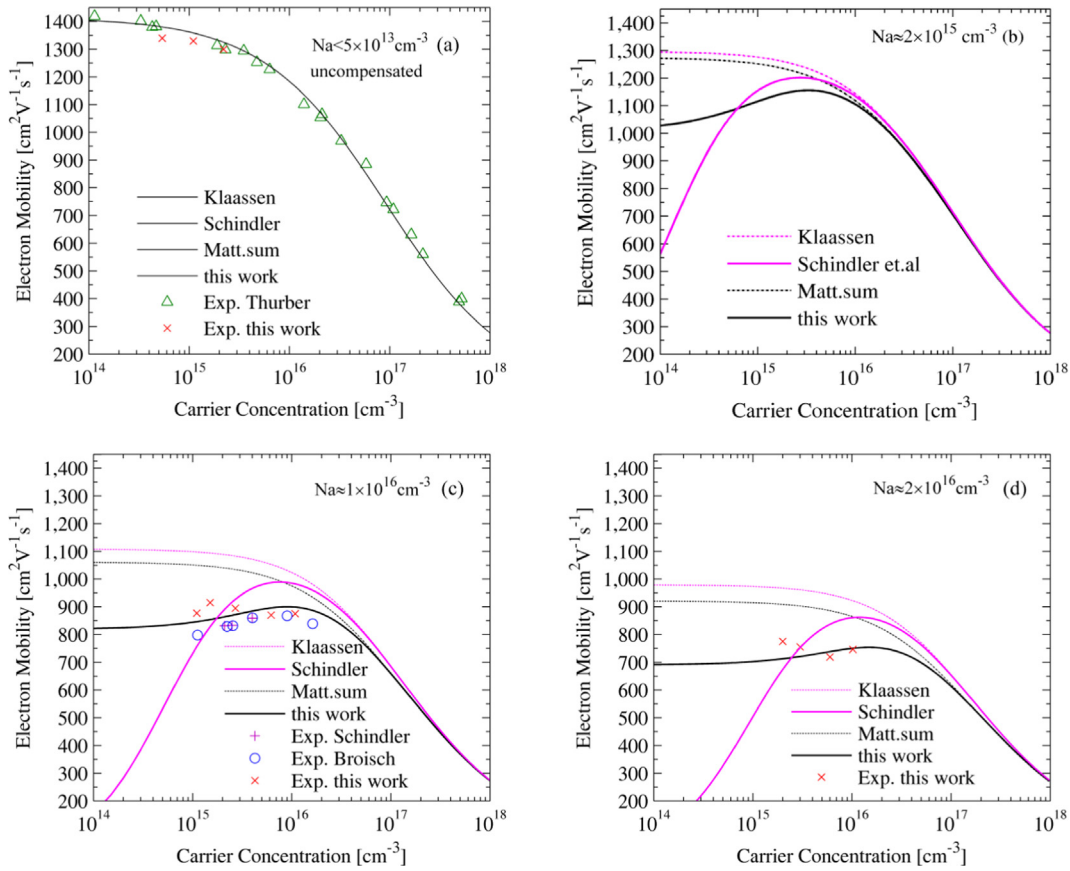
Fig. 2. Evolutions of majority electron mobility when concentrations of boron are fixed at (a) Na < 5 × 10^{13} cm^{-3} (uncompensated silicon); (b) Na ≈ 2.0 × 10^{15} cm^{-3}; (c) Na ≈ 1.0 × 10^{16} cm^{-3}; (d) Na ≈ 2.0 × 10^{16} cm^{-3}. Some of the measured electron mobilities are from publications by Schindler et al. [16], Broisch et al. [1] and Thurber et al. [38].

where $\mu_{e,D}(N_D, c)$ is electron mobility due to donor scattering; $\mu_{e,A}(N_A, c)$ is electron mobility due to acceptor scattering; $\mu_{e,h}(p, c)$ is electron mobility due to hole scattering. The c and p are concentrations of electrons and holes, respectively.

Finally, the calculated total electron mobility in the n-type compensated silicon following Matthiesen's rule, which is based on the basic equations in Klaassen's work [8], is expressed as follows:

$$\mu_{e,Matt.sum}^{-1} = \mu_{e,D}^{-1} + \left[\mu_{e,D}(N_D = N_A, c)/G(P)\right]^{-1}$$
$$+ \left[F(P)\mu_{e,D}(N_D = p, c)\right]^{-1} + \mu_{e,L}^{-1} \tag{8}$$

Similarly, the calculated total hole mobility in the n-type compensated silicon following Matthiesen's rule, which is based on the basic equations in Klaassen's work [8], is expressed as follows:

$$\mu_{h,Matt.sum}^{-1} = \mu_{h,D}^{-1} + \left[\mu_{h,A}(N_A = N_D, c)/G(P)\right]^{-1}$$
$$+ \left[F(P)\mu_{h,A}(N_A = c, c)\right]^{-1} + \mu_{h,L}^{-1} \tag{9}$$

Instead of using Klaassen's unified model $\mu_{i,Klaassen}(i = e, h)$, the calculated $\mu_{i,Matt.sum}(i = e, h)$ by the above basic equations (Eqs. (8) and (9)) is closer to measured data as shown in Figs. 2 and 3. In this way, the deviations which originate from the above-mentioned first reason are avoided. Yet, as the calculated $\mu_{i,Matt.sum}$ still shows slight deviations from measured data (see Figs. 2 and 3), a correction term which is related to the reduced screening effect (the second reason) has to be considered in our calculation.

3.1.2.2. Correction term with no additional parameters included. Carrier mobilities due to different scatterings are expressed using a similar equation as Eq. (2). Since the second term on the right hand side of Eq. (2) stems via statistical screening by majority carriers, it is in principle inappropriate for carriers to screen the repulsive ionized potentials (e.g. electron carriers for repulsive ionized acceptors and holes). Therefore, the inappropriate screening effect on repulsive ionized potentials can be calculated and summed up following the Matthiesen's rule. In this way, we propose a correction term with the weighing factors of minority impurity scattering G (P), carrier scattering F(P), and term for reduced screening $\mu_{i,c}\Delta c/N_{maj.}$ (here Δc equals the concentration of compensated minority impurities, i.e. $\Delta c = N_{min.}$), and it reads:

$$\mu_{i,corr.} = \mu_{i,c}\alpha\left(\frac{N_{min.}}{N_{maj.}}\right)^{\beta}\left[G(P) + \frac{1}{F(P)}\right] \tag{10}$$

where the subscript i stands for e (electrons) or h (holes); the value of $\mu_{i,c}$ is consistent with the basic Caughey-Thomas expression [37] (see also Ref. [9]); α is fitted to 1; β is fitted to 1.6 based on a large number of published and our measured carrier mobilities on both n- and p-type compensated silicon. $N_{maj.}$ and $N_{min.}$ are concentrations of majority impurities and minority impurities, respectively.

As derived from Eq. (2), it follows the statistical screening theory by Ridley that the term for screening should be treated on the right side, i.e. $\mu_{i,Matt.sum} = \mu_{i,Optimized} + \mu_{i,corr.}$. Thus, the decrease of carrier mobility caused by reduced screening ($\mu_{i,corr.}$) is subtracted from the total carrier mobility calculated by Eqs. (8) and (9), which reads:

$$\mu_{i,Optimized} = \mu_{i,Matt.sum} - \mu_{i,corr.} \tag{11}$$
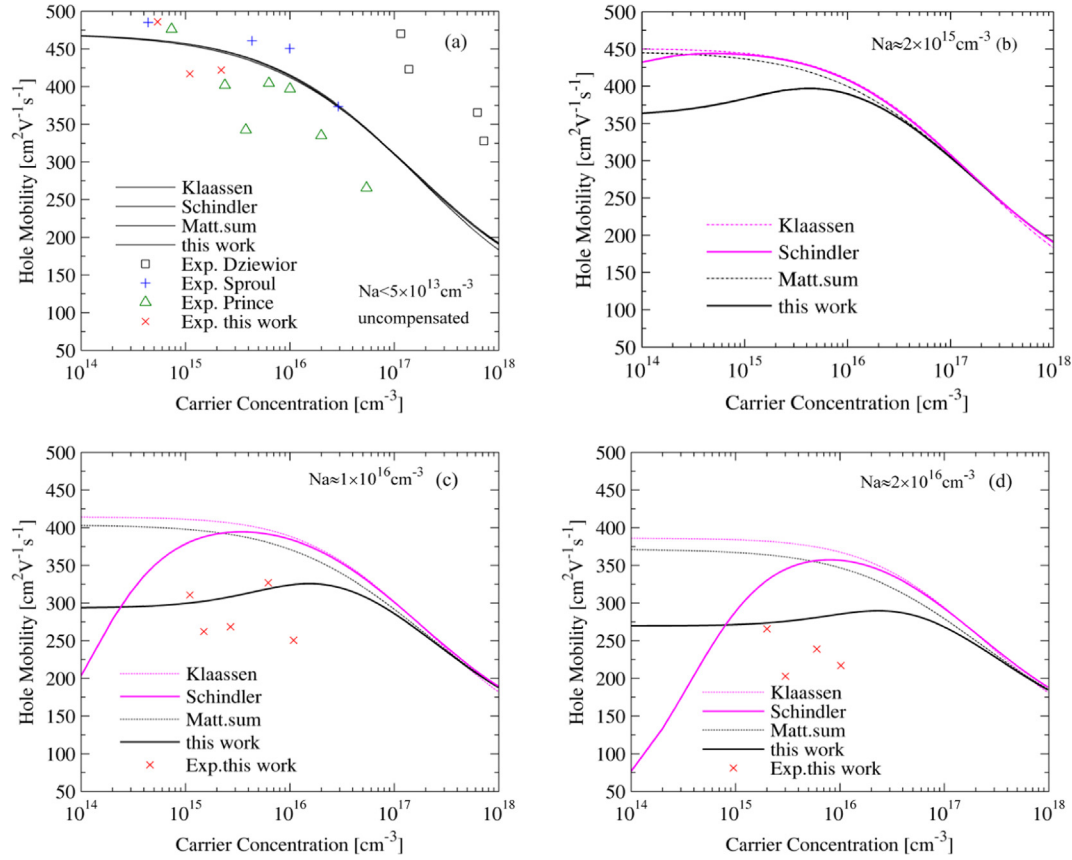
Fig. 3. Evolutions of minority hole mobility when the concentration of boron is fixed at (a) Na < 5 × 10^13 cm^−3 (uncompensated silicon); (b) Na ≈ 2.0 × 10^15 cm^−3; (c) Na1.0 × 10^16 cm^−3; (d) Na2.0 × 10^16 cm^−3. Some of the measured hole mobilities are from publications by Dziewior and Silber [39], Sproul et al. [40] and Prince [41].

In case of electron mobility in the n-type compensated silicon, the total carrier mobility calculated by our optimized model is expressed as:

$$
\mu_{e,Optimized} = \left\{ \mu_{e,D}^{-1} + \left[\mu_{e,D}(N_D = N_A, c)/G(P) \right]^{-1} \right.
$$
$$
+ \left[F(P)\mu_{e,D}(N_D = p, c) \right]^{-1} + \mu_{e,L}^{-1} \left. \right\}^{-1}
$$
$$
- \mu_{i,c} \left(\frac{N_A}{N_D} \right)^{1.6} \left[G(P) + \frac{1}{F(P)} \right] \tag{12}
$$

Consequently, as illustrated by dark curve lines in Figs. 2 and 3, the calculated carrier mobilities by our optimized model in this work $\mu_{i,Optimized}$ are better fitted to the measured data than Klaassen's model. Further investigation is needed to explain the physics behind this correction term, but this optimized model has already enabled us to predict the carrier mobility in the compensated silicon with a good accuracy (as evaluation of the optimized model in the next subsection).

3.1.3. Evaluation of the optimized model by calculating relative deviations

In this subsection, Klaassen's unified model and our optimized model are compared for various concentrations of boron in the n-type compensated silicon by calculating relative deviations from measured mobilities. The relative deviation is defined as $(\mu_{i,Exp.} - \mu_{i,cal.})/\mu_{i,Exp.}$, where the subscript i stands for e for electrons and h for holes; cal. stands for Klaassen' model and the optimized model in this work. The relative deviations of calculated electron and hole mobilities by Klaassen's model from experimental mobilities are illustrated in Figs. 4 and 5(a), respectively. Reductions of

−65% − 5% of majority electron mobility from Klaassen's model are observed as shown in Fig. 4(a). Similarly, an average reduction of −60% of experimental hole mobility from Klaassen's model is observed as shown in Fig. 5(a).

Both electron and hole mobilities are calculated by our optimized model as Eq. (11) at given concentrations of impurities. Relative deviations of electron mobilities calculated by our optimized model from experimental electron mobilities are illustrated in Fig. 4(b), and maximum relative deviations of 20% and −10% are observed, which are acceptable uncertainties of measurements. It is noted that the negative and positive deviations are due to the uncertainties of dopant and carrier concentration measurements. Relative deviations of hole mobilities calculated by our optimized model from experimental hole mobilities, which range from −20% and 20%, are illustrated in Fig. 5(b). It is noted that these deviations are mainly due to the uncertainties of measurement of carrier concentration, carrier diffusion length and carrier lifetime, and that the maximum deviations are from carrier mobilities measured on boron, phosphorus, and gallium co-doped and thermal donor activated samples. Excellent agreements between measured carrier mobilities and our optimized model are obtained. It is noteworthy that the parameters in our optimized model are consistent with Klaassen's model at room temperature.

It needs to be mentioned that the minority dopants (e.g. boron in the n-type compensated silicon) are 100% ionized and that the ionization ratio of majority dopants is only slightly lower (e.g. the majority phosphorus in the n-type compensated silicon is 99.6% ionized with a net doping concentration of 1×10^{16} cm^−3 calculated by Altermatt et al. [45]). Thus, although incomplete ionization is not considered in this work, the resulting small deviation
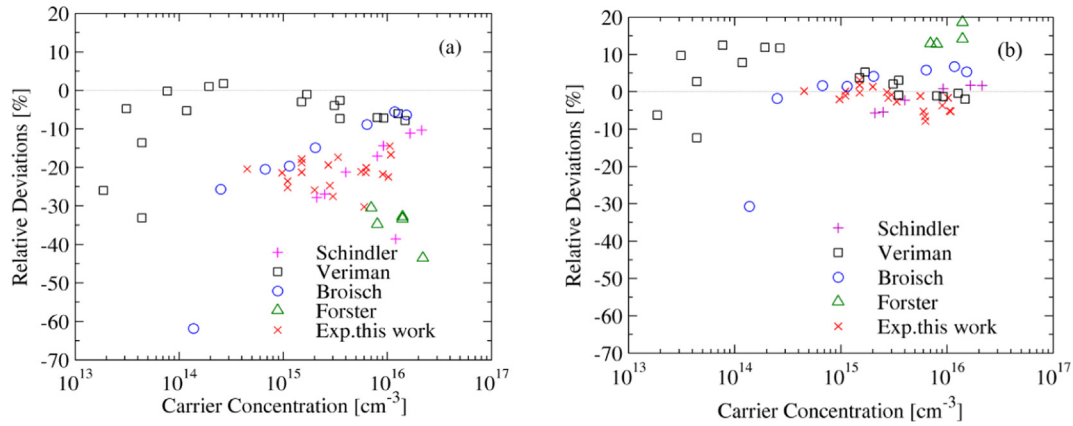
Fig. 4. Relative deviations of measured electron mobilities on the n-type compensated silicon from Klaassen's model are illustrated in (a); and relative deviations of measured electron mobilities on the n-type compensated silicon from the optimized model are illustrated in (b). Some of the measured electron mobilities are from publications by Schindler et al. [16], Veirman et al. [4], Broisch et al. [1], and Forster [11].
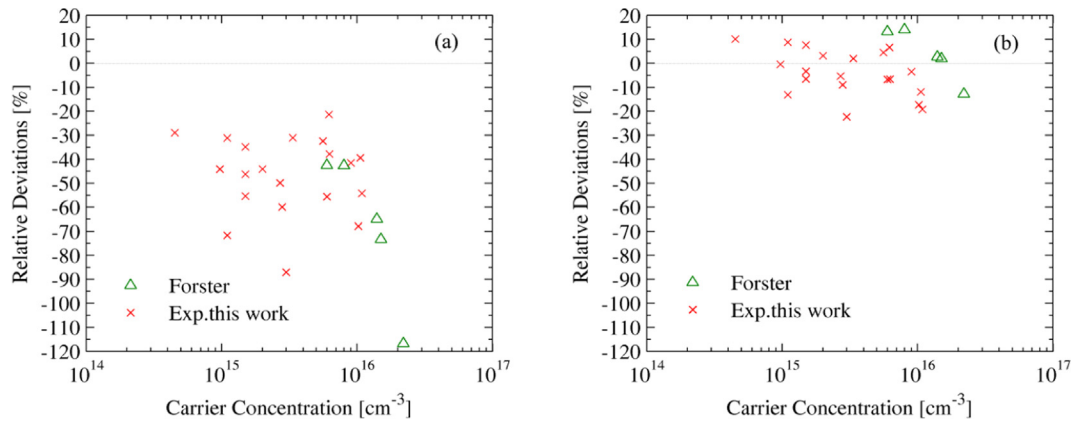
Fig. 5. Relative deviations of measured hole mobilities on the n-type compensated silicon from Klaassen's model are illustrated in (a); and relative deviations of measured hole mobilities on the n-type compensated silicon from the optimized model are illustrated in (b). Some of the measured hole mobilities are from publication by Forster [11].

is negligible for our calculation. In addition, about temperature dependence of carrier mobility in the compensated silicon, Klaassen suggested using CW-BH approach (temperature dependence of $\mu_{i,N}$ and $\mu_{i,c}$ can be found in Eqs. (2a) and (2b) in Ref. [10]). Similarly, as we use the same parameters as Klaasen's model (e.g. $\mu_{i,N}$ and $\mu_{i,c}$ in Eq. (2), and $\mu_{i,c}$ in the correction term), our suggested optimized model should follow the same temperature dependence of Klaassen. More experimental work is still needed to investigate the temperature dependence of the optimized model.

3.2. Model extended for p-type compensated silicon

When it comes to p-type compensated silicon, carrier mobilities are also calculated by our optimized model as depicted in Eq. (11). Relative deviations of majority hole mobilities measured on the p-type compensated silicon wafers from Klaassen's model and from the optimized model are calculated. Large reductions of measured hole mobilities from Klaassen's model are also observed for the p-type compensated silicon as illustrated in Fig. 6(a). The minority impurity (phosphorus) in the p-type compensated silicon induces new impurity scattering and reduced screening effect, which has been completely considered by the optimized model as depicted by Eq. (11). Therefore, as shown in Fig. 6(b), the optimized model shows a good agreement with measured hole mobilities on the p-type compensated silicon (the calculated relative deviations of
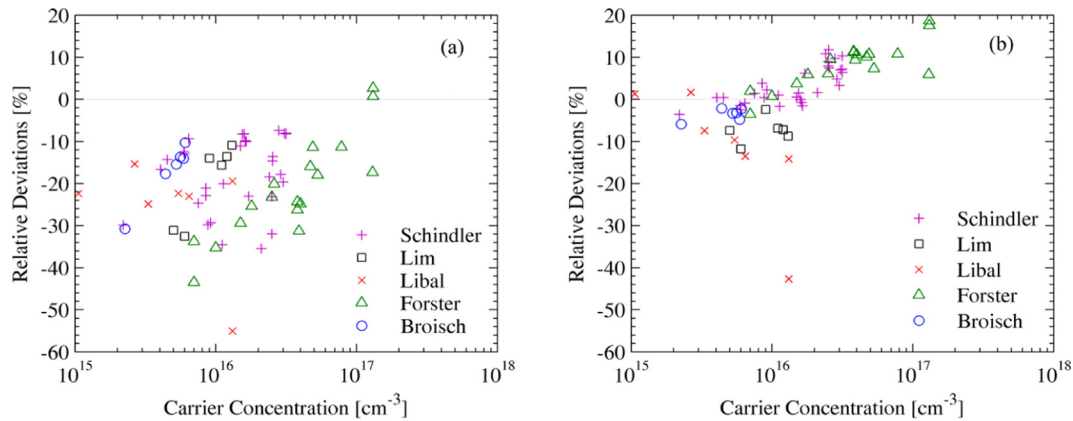
measured hole mobilities by our optimized model range from −15% and 15% as illustrated in Fig. 6(b).

4. Simulated and experimental results along with the crystal length

Two silicon crystal rods (Cz0 and Cz1) are grown by Cz method under identical conditions except the concentrations of dopants. The feedstock of Cz0 is the n-type compensated silicon while the feedstock of Cz1 is the uncompensated silicon. The initial concentrations of main impurities in silicon feedstock for both Cz0 and Cz1 are listed in Table 1. Since the feedstock of Cz1 is made from Siemens method, phosphorus is added to control the starting resistivity at about 3.5 Ω cm. The total length of both crystal rods is about 150 cm, and measurement of resistivity is on the wafer level. Since the bulk concentration of oxygen is high in Cz silicon, a thermal donor annihilation has been carried out. Regarding Ge and C in Cz1, they have no apparent influence on the electrical properties of silicon [46-48].

4.1. Profile of resistivity

The resistivity is calculated by $\rho = 1/cq\mu_e$, where c equals to $N_D - N_A$. Hence, in the compensated silicon, the evolution of resistivity is determined by the competition between donor and acceptor concentrations as crystal grows. Concentrations of donor (N_D)

Fig. 6. Relative deviations of measured hole mobilities on the p-type compensated silicon from Klaassen's model are illustrated in (a); and relative deviations of measured hole mobilities on the p-type compensated silicon from the optimized model are illustrated in (b). Some of the measured hole mobilities are from publications by Schindler et al. [16], Lim et al. [6], Libal et al. [14], Forster [11], and Broisch et al. [1].

Table 1
Initial concentrations of main impurities in silicon feedstock.

	B (cm^{-3})	P (cm^{-3})	Ge (cm^{-3})	C (cm^{-3})	O (cm^{-3})
Cz0	1.1×10^{16}	3.05×10^{16}	5.1×10^{16}	2.2×10^{17}	2.0×10^{17}
Cz1[a]	$< 2 \times 10^{14}$	$< 2 \times 10^{14}$	$< 2 \times 10^{14}$	$< 4 \times 10^{16}$	$< 1 \times 10^{17}$

[a] The concentration of impurities in Cz1 is referred as statements of silicon manufacturer.

and acceptor (N_A) are calculated as crystal grows using Scheil equation [49] with effective segregation coefficients of 0.81 and 0.36, respectively (these two effective segregation coefficients are calculated by BPS theory for Cz1 and Cz0 [50]). Electron mobilities μ_e are both calculated by Klaassen's model and the optimized model, respectively, in this work. Accordingly, the obtained resistivities using electron mobilities calculated by these two models are plotted in Fig. 7. Fig. 7 also shows our measured resistivities on the uncompensated Cz0 and compensated Cz1.

It is very interesting to note that the tendency curves of resistivity for the uncompensated silicon are convex and that the tendency curves gradually transfer to concave as the minority impurity (i.e. boron in the n-type compensated silicon) increases. The deviations of measured resistivities from calculated resistivities by Klaassen's model are very large at the beginning of crystal

growth. This is because the overestimated electron mobilities by Klaassen's model lead to lower calculated resistivities at the beginning of crystal growth. As illustrated in Fig. 7, the calculated blue curve of resistivities using electron mobilities predicted by our optimized model is better fitted to measured resistivities. As a consequence, our optimized model gives more accurate carrier mobility prediction than Klaassen's model for the n-type compensated silicon.

4.2. Profile of minority hole mobility

Measured hole mobilities of wafers from uncompensated Cz0 and compensated Cz1 are plotted in Fig. 8 as crystal grows. Evolutions of hole mobilities are calculated by these two models (Klaassen's model and the optimized model) with segregated
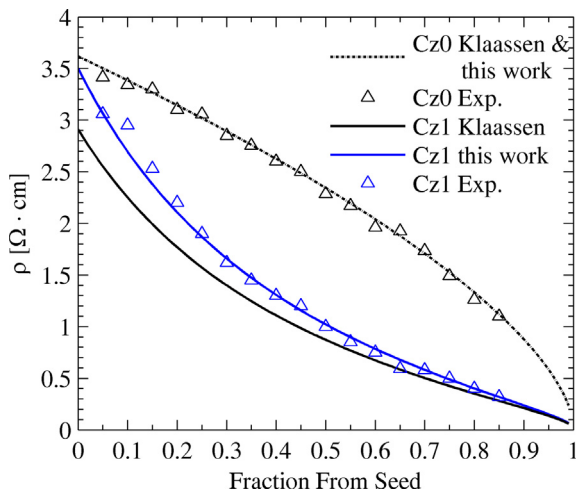
Fig. 7. Resistivities of both uncompensated Cz0 and compensated Cz1 are predicted using electron mobilities calculated by two models (i.e. Klasssen's model and the optimized model). Measured resistivities of Cz0 and Cz1 are also plotted.
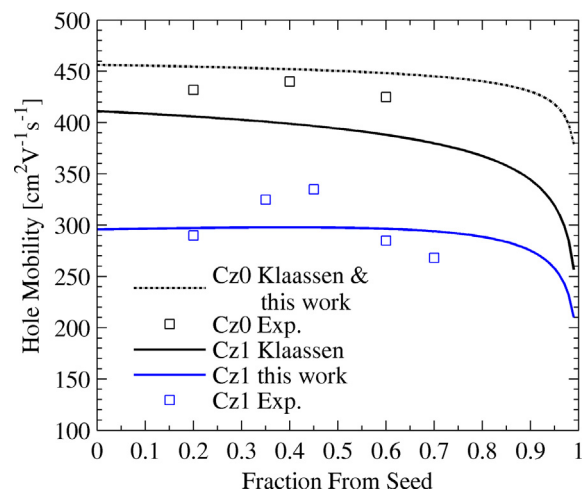
Fig. 8. Hole mobilities of both uncompensated Cz0 and compensated Cz1 are calculated by two models (i.e. Klaassen's model and the optimized model). Measured hole mobilities are also plotted.

concentrations of donor (N_D) and acceptor (N_A) along with the crystal length. One can see that hole mobilities of the compensated Cz1 are evidently lower than those of the uncompensated Cz0. This can be explained by the additional minority impurity scattering in the compensated Cz1. As shown in Fig. 8, the hole mobilities are rather uniformly distributed along with the crystal length, irrespective of varied net doping concentration. Since the carrier concentration of Cz1 is lower than 1×10^{16} cm^{-3} ($\rho > 0.5 \Omega$ cm) for most of the crystal (fraction < 0.9), the moving carrier scattering is not as significant as the fixed impurity scattering for the compensated Cz1. In addition, our optimized model is better fitted to measured hole mobilities on the compensated Cz1 than Klaassen's model.

5. Conclusion

Both electron and hole mobilities measured on the n-type compensated solar-grade silicon wafers are presented in this paper. To give accurate prediction of carrier mobilities in the n-type compensated silicon, the discrepancy between Klaassen's model and measured carrier mobilities is analyzed in detail. It is found that the large discrepancy is not only due to the reduced screening but also due to the inappropriate parameters of Klaassen's model when it is applied to the compensated silicon.

We present an optimized model with no additional parameters included, which agrees well with previously published and our measured carrier mobilities. In our optimized model, carrier mobilities due to different scatterings are summed up following the basic Matthiesen's rule, and then a correction term related to a reduced screening is subtracted. In addition, the optimized model in this work also agrees well with measured carrier mobilities when we extend it to the p-type compensated silicon.

We also investigate the evolution of carrier mobilities along with the crystal length in the n-type compensated Cz silicon. It is concluded that the reduction of electron mobility by compensation leads to higher resistivity at the beginning of crystal growth of the n-type compensated silicon. The minority hole mobility shows very uniform distribution along with the crystal length for the n-type compensated Cz silicon, which implies that the reduction of hole mobilities is mainly due to additional impurity scattering other than the carrier scattering.

Acknowledgments

Appendix A. Supplementary material

Supplementary data associated with this article can be found, in the online version, at http://dx.doi.org/10.1016/j.jcrysgro.2017.07.018.

References

[1] J. Broisch, F. Schindler, M.C. Schubert, F. Fertig, A.K. Soiland, S. Rein, IEEE J. Photovolt. 5 (2015) 1276.
[2] D. Macdonald, L. Geerligs, Appl. Phys. Lett. 85 (2004) 4061.
[3] M. Forster, F.E. Rougieux, A. Cuevas, B. Dehestru, A. Thomas, E. Fourmond, M. Lemiti, IEEE J. Photovolt. 3 (2013) 108.
[4] J. Veirman, S. Dubois, N. Enjalbert, J.P. Garandet, D.R. Heslinga, M. Lemiti, Solid State Electron 54 (2010) 671.
[5] F. Rougieux, D. Macdonald, A. Cuevas, S. Ruffell, J. Schmidt, B. Lim, A. Knights, J. Appl. Phys. 108 (2010) 013706.
[6] B. Lim, M. Wolf, J. Schmidt, Phys. Status Solidi (c) 8 (2011) 835.
[7] S. Zhang, C. Modanese, M.D. Sabatino, G. Tranell, J. Cryst. Growth 429 (2015) 43.
[8] D.B.M. Klaassen, Solid State Electron 35 (1992) 953.
[9] D.B.M. Klaassen, Solid State Electron 35 (1992) 961.
[10] F. Rougieux, D. MacDonald, A. Cuevas, Prog. Photovoltaics 19 (2011) 787.
[11] M. Forster, Ph.D. thesis, INSA de Lyon, 2012.
[12] P.P. Altermatt, J. Comput. Electron 10 (2011) 314.
[13] F. Schindler, M.C. Schubert, A. Kimmerle, J. Broisch, S. Rein, W. Kwapil, W. Warta, Sol. Energy Mater. Sol. Cells 106 (2012) 31.
[14] J. Libal, S. Novaglia, M. Acciarri, S. Binetti, R. Petres, J. Arumughan, R. Kopecek, A. Prokopenko, J. Appl. Phys. 104 (2008) 104507.
[15] C. Xiao, D. Yang, X. Yu, P. Wang, P. Chen, D. Que, Sol. Energy Mater. Sol. Cells 101 (2012) 102.
[16] F. Schindler, M. Forster, J. Broisch, J. Schön, J. Giesecke, S. Rein, W. Warta, M.C. Schubert, Sol. Energy Mater. Sol. Cells 131 (2014) 92.
[17] E. Fourmond, M. Forster, R. Einhaus, H. Lauvray, J. Kraiem, M. Lemiti, Energy Proc. 8 (2011) 349.
[18] M. Forster, A. Cuevas, E. Fourmond, F.E. Rougieux, M. Lemiti, J. Appl. Phys. 111 (2012) 043701.
[19] F. Jay, D. Muñoz, T. Desrues, E. Pihan, V. Amaral de Oliveira, N. Enjalbert, A. Jouini, Sol. Energy Mater. Sol. Cells 130 (2014) 690.
[20] P. Zheng, F.E. Rougieux, C. Samundsett, X. Yang, Y. Wan, J. Degoulange, D. Macdonald, Appl. Phys. Lett. 108 (2016) 122103.
[21] T. Surek, J. Cryst. Growth 275 (2005) 292.
[22] P. Krenckel, S. Riepe, F. Schindler, T. Strauch, J. Cryst. Growth 463 (2017) 145.
[23] A. Lanterne, G. Gaspar, Y. Hu, E. Øvrelid, M.D. Sabatino, J. Cryst. Growth 458 (2017) 120.
[24] J.A. Silva, B. Platte, M.C. Brito, J.M. Serra, J. Cryst. Growth 428 (2015) 29.
[25] R. Einhaus, J. Kraiem, F. Cocco, Y. Caratini, D. Bernou, D. Sarti, G. Rey, R. Monna, C. Trassy, J. Degoulange, Proceedings of the 21st European PVSEC, 580, 2006.
[26] Y. Delannoy, J. Cryst. Growth 360 (2012) 61.
[27] S. S. Pascoa, Master Thesis, Norwegian University of Science and Technology, Trondheim, 2014.
[28] U. Gösele, T.Y. Tan, Appl. Phys. A 28 (1982) 79.
[29] Eiji Ohta, M. Sakata, Jpn. J. Appl. Phys. 17 (1978) 1795.
[30] F. Szmulovicz, Phys. Rev. B 34 (1986) 4031.
[31] Leeor Kronik, Y. Shapira, Surf. Interf. Anal. 31 (2001) 954.
[32] K. Kirilov, V. Donchev, T. Ivanov, K. Germanova, P. Vitanov, P. Ivanov, J. Optoelectron. Adv. M. 7 (2005) 533.
[33] M. Wilson, A. Savtchouk, F. Buchholz, S. Olibet, R. Kopecek, K. Peter, J. Lagowski, 26th European Photovoltaics Solar Energy Conference and Exhibition Hamburg, 979, 2011.
[34] D. Chattopadhyay, H.J. Queisser, Rev. Mod. Phys. 53 (1981) 745.
[35] Albert Messiah, G.M. Temmer, Science 136 (1962).
[36] R.B. Bernstein, A. Dalgarno, H. Massey, I.C. Percival, P. Roy. Soc. A 274 (1963) 427.
[37] G. Masetti, M. Severi, S. Solmi, IEEE T. Electron Dev. 30 (1983) 764.
[38] W.R. Thurber, R.L. Mattis, Y.M. Liu, J.J. Filliben, Final Report National Bureau of Standards Washington Dc, 42, 1981.
[39] J. Dziewior, D. Silber, Appl. Phys. Lett. 35 (1979) 170.
[40] A.B. Sproul, M.A. Green, A.W. Stephens, J. Appl. Phys. 72 (1992) 4161.
[41] B. Prince, Phys. Rev. 93 (1954) 1204.
[42] B.K. Ridley, J. Phys. C Solid State Phys. 10 (2001).
[43] D.M. Caughey, R.E. Thomas, P. IEEE 55 (1967) 2192.
[44] B.K. Ridley, Quantum Process. Semiconduct. 34 (2013) 251.
[45] P.P. Altermatt, A. Schenk, G. Heiser, J. Appl. Phys. 100 (2006) 113714.
[46] J.C.Å. Lilliestråle, Master Thesis, Norwegian University of Science and Technology, Trondheim, 2012.
[47] T. Nozaki, Y. Yatsurugi, N. Akiyama, J. Electrochem. Soc. 117 (1970) 1566.
[48] Y. Wu, S. Yuan, X. Yu, X. Qiu, H. Zhu, J. Qian, D. Yang, Sol. Energy Mater. Sol. Cells 154 (2016) 94.
[49] Erich Scheil, Zeitschrift für Metallkunde 34 (1942) 70.
[50] J.A. Burton, R.C. Prim, W.P. Slichter, J. Chem. Phys. 21 (1953) 1987.